Eur. Phys. J. A (2012) **48**: 29
DOI 10.1140/epja/i2012-12029-2

THE EUROPEAN PHYSICAL JOURNAL A

Tools for Experiment and Theory

Simultaneous measurement of neutron-induced capture and fission reactions at CERN

C. Guerrero[1,2a], E. Berthoumieux[1,7], D. Cano-Ott[2], E. Mendoza[2], S. Andriamonje[1], J. Andrzejewski[4], L. Audouin[3], M. Barbagallo[10], V. Bécares[2], F. Bečvář[5], F. Belloni[6], J. Billowes[26], M. Brugger[1], M. Calviani[1], F. Calviño[8], C. Carrapiço[9], F. Cerutti[1], E. Chiaveri[1], M. Chin[1], N. Colonna[10], G. Cortés[8], M.A. Cortés-Giraldo[11], M. Diakaki[25], I. Dillmann[12], C. Domingo-Pardo[13], I. Duran[14], C. Eleftheriadis[28], M. Fernández-Ordóñez[2], A. Ferrari[1], S. Ganesan[15], G. Giubrone[16], M.B. Gómez-Hornillos[8], I.F. Gonçalves[9], E. González-Romero[2], F. Gramegna[17], E. Griesmayer[18], F. Gunsing[7], D. Jenkins[27], E. Jericha[18], Y. Kadi[1], F. Käppeler[18], D. Karadimos[25], J. Kroll[5], M. Krtička[5], E. Lebbos[1], C. Lederer[20], H. Leeb[18], R. Losito[1], M. Lozano[11], A. Manousos[28], J. Marganiec[2], S. Marrone[10], T. Martinez[2], C. Massimi[21], P.F. Mastinu[17], M. Meaze[10], A. Mengoni[22], P.M. Milazzo[6], C. Paradela[14], A. Pavlik[20], J. Perkowski[4], R. Plag[13], J. Praena[11], J.M. Quesada[11], T. Rauscher[23], R. Reifarth[13], F. Roman[1,24], C. Rubbia[1], R. Sarmento[9], G. Tagliente[10], J.L. Tain[16], D. Tarrío[14], L. Tassan-Got[3], A. Tsinganis[251], G. Vannini[21], V. Variale[10], P. Vaz[9], A. Ventura[22], M. Vermeullen[27], V. Vlachoudis[1], R. Vlastou[25], A. Wallner[20], T. Ware[26], C. Weiß[18], and T. Wright[26]

[1] European Organization for Nuclear Research (CERN), Geneva, Switzerland
[2] Centro de Investigaciones Energéticas Medioambientales y Technológicas (CIEMAT), Madrid, Spain
[3] Centre National de la Recherche Scientifique/IN2P3 - IPN, Orsay, France
[4] Uniwersytet Łódzki, Lodz, Poland
[5] Charles University, Prague, Czech Republic
[6] Istituto Nazionale di Fisica Nucleare, Trieste, Italy
[7] Commissariat à l'Énergie Atomique (CEA) Saclay - Irfu, Gif-sur-Yvette, France
[8] Universitat Politècnica de Catalunya, Barcelona, Spain
[9] Instituto Tecnológico e Nuclear (ITN), Lisbon, Portugal
[10] Istituto Nazionale di Fisica Nucleare, Bari, Italy
[11] Universidad de Sevilla, Sevilla, Spain
[12] Physik Department E12 and Excellence Cluster Universe, Technische Universität München, Munich, Germany
[13] GSI Helmholtzzentrum für Schwerionenforschung GmbH, Darmstadt, Germany
[14] Universidade de Santiago de Compostela, Spain
[15] Bhabha Atomic Research Centre (BARC), Mumbai, India
[16] Instituto de Física Corpuscular, CSIC-Universidad de Valencia, Spain
[17] Istituto Nazionale di Fisica Nucleare, Laboratori Nazionali di Legnaro, Italy
[18] Atominstitut, Technische Universität Wien, Austria
[19] Karlsruhe Institute of Technology, Campus Nord, Institut für Kernphysik, Karlsruhe, Germany
[20] University of Vienna, Faculty of Physics, Austria
[21] Dipartimento di Fisica, Università di Bologna and INFN, Sezione di Bologna, Bologna, Italy
[22] Agenzia nazionale per le nuove tecnologie, l'energia e lo sviluppo economico sostenibile (ENEA), Bologna, Italy
[23] Department of Physics and Astronomy - University of Basel, Basel, Switzerland
[24] Horia Hulubei National Institute of Physics and Nuclear Engineering - IFIN HH, Bucharest - Magurele, Romania
[25] National Technical University of Athens (NTUA), Greece
[26] University of Manchester, UK
[27] University of York, UK
[28] Aristotle University of Thessaloniki, Thessaloniki, Greece

Received: 21 December 2011 / Revised: 7 February 2012
Published online: 12 March 2012 –
Communicated by R. Krücken

Abstract. The measurement of the capture cross-section of fissile elements, of utmost importance for the design of innovative nuclear reactors and the management of nuclear waste, faces particular difficulties related to the γ-ray background generated in the competing fission reactions. At the CERN neutron time-of-flight facility n_TOF we have combined the Total Absorption Calorimeter (TAC) capture detector with a set of three ^{235}U loaded MicroMegas (MGAS) fission detectors for measuring simultaneously two reactions: capture and fission. The results presented here include the determination of the three detection efficiencies involved in the process: $\varepsilon_{TAC}(n,f)$, $\varepsilon_{TAC}(n,\gamma)$ and $\varepsilon_{MGAS}(n,f)$. In the test measurement we have succeeded in measuring simultaneously with a high total efficiency the ^{235}U capture and fission cross-sections, disentangling accurately the two types of reactions. The work presented here proves that accurate capture cross-section measurements of fissile isotopes are feasible at n_TOF.

[a] e-mail: carlos.guerrero@cern.ch

1 Introduction

The measurement of accurate neutron-induced capture and fission cross-sections is essential for the design of innovative nuclear systems such as ADS and Gen-IV reactors [1,2]. Out of all the neutron-induced cross-sections that play a role in nuclear technology applications, those for which improvement is considered of utmost importance are included in the *High Priority Request List* [3] of the *International Atomic Energy Agency* IAEA. This list is continuously updated by the *Nuclear Energy Agency* (NEA). Half of the capture cross-section measurements included in this list (^{nat}Hf, ^{233,235,238}U, ^{239,241,242}Pu, ^{241}Am) are of fissile isotopes, and these are very difficult to measure because in such cases the γ-rays generated in fission reactions may constitute a very large background when measuring γ-rays emitted in neutron capture reactions.

The measurement of neutron-induced cross-sections of actinides is one of the scientific goals of the n_TOF Collaboration. Thanks to the unique characteristics of the n_TOF facility [4] at CERN, valuable capture and fission cross-section data have been measured since 2002. Figure 1 shows the neutron capture measurements of actinides performed at n_TOF-Ph1 (^{233,234}U, ^{237}Np, ^{240}Pu and ^{243}Am [5]) and those intended for n_TOF-Ph2 (^{236,238}U and ^{241}Am [6]), some of which are being or have been measured since 2010. Among all those already measured, only ^{233}U is fissile; meaning that below the characteristic fission threshold the fission cross-section is very small and does not compete with the neutron capture or scattering reactions. The results from capture measurements of non-fissile isotopes at n_TOF have reached an accuracy better than 4%. However, in the case of ^{233}U and due to the background from fission reactions the accuracy was limited to only 10% [7]. Such an accuracy is remarkable with respect to previous measurements, but still not sufficient for some actinides taking into account the nuclear data requirements in the field of nuclear technologies.

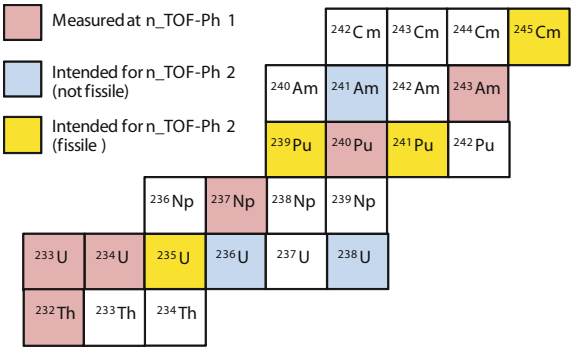

Fig. 1. Minor actinide part of the table of isotopes. Details on the isotopes measured already at n_TOF-Ph1 and those intended in the present n_TOF-Ph2, differentiating between fissile and non-fissile isotopes.

In consideration of the importance of measuring the capture cross-section of fissile isotopes with high accuracy we have designed, built and tested a new set-up that would allow us to achieve such goal. The new set-up consists of the combination of the Total Absorption Calorimeter (TAC) [8] with a MicroMegas (MGAS) [9] fission detector. This new set-up has been used to measure simultaneously the capture and fission cross-sections of ^{235}U using a stack of three thin ^{235}U samples (see [10] for a set-up at LANL tested for a similar purpose).

2 Experimental set-up

At the n_TOF neutron *time-of-flight* (TOF) facility neutrons are generated in spallation reactions by a pulsed proton beam of $7{\cdot}10^{12}$ protons per pulse with 20 GeV/c momentum impinging on a cylindrical lead block (60 cm in diameter and 40 cm in length) surrounded by water (1 cm). Neutrons are moderated by adding a 4 cm thick borated water (mixed with 1.28% of boric acid, 96% enriched in ^{10}B) layer. The neutron beam reaching the measuring station at 185 m ranges from relativistic (TOF = 617 ns) to subthermal (TOF > 84 ms) neutron energies. The measurement of the neutron-induced reactions, in this case for both the capture and fission reactions on ^{235}U, as a function of their TOF allows one to determine the associated cross-sections as a function of neutron energy. At n_TOF, the TOF is always measured with respect to the *Current Monitor* (PKUP) placed in the proton beam line just upstream for the spallation target.

The measurement combines two detectors that have been used independently in previous n_TOF campaigns: the Total Absorption Calorimeter (TAC) [8] and three MicroMegas (MGAS) detectors [9].

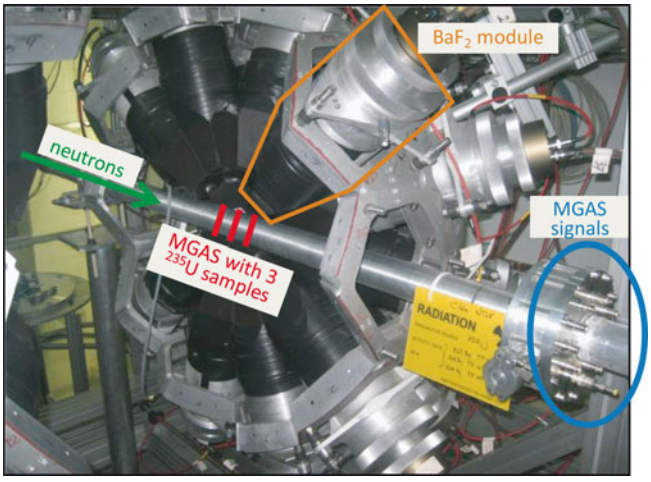

Fig. 2. Picture of one hemisphere of the 4π Total Absorption Calorimeter (TAC) and the long gas chamber inserted along its axis. The picture includes labels indicating the direction of the neutron beam, the position of the three MGAS detectors, the individual crystals, and the connexions for cables. The spherical neutron absorber (see ref. [8]) was used but it is not shown in this picture.

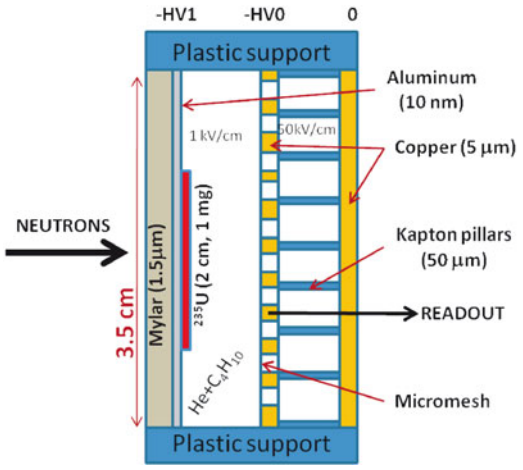

Fig. 3. Sketch of one MicroMegas (MGAS) detector loaded with a ^{235}U sample (not to scale).

The TAC is a segmented 4π detector made of 40 BaF_2 crystals of 15 cm in thickness (see fig. 2). The detector was specifically designed and built for fully detecting with high efficiency the γ-ray cascades following neutron capture reactions, with typical total energies of 5–10 MeV and multiplicities that may range up to 6 or 8, depending on the investigated nucleus. The signals from the 40 BaF_2 crystals are directly connected to 8 bit flash-ADC digitizers (with 8 MB memory per channel) sampling at 250 MHz, which allow recording 32 ms long data buffers that cover the neutron energy range from relativistic energies down to 0.3 eV.

The MGAS, based on the microbulk principle, is a very particular gas detector with an active volume divided in two regions by a thin micromesh (see fig. 3). The ionization produced by the fission fragments from ^{235}U takes place in the first region (4 mm, $\sim$ 1 kV/cm) and the electrons produced are multiplied by producing an avalanche in the second region (50 μm, $\sim$ 50 kV/cm), thus amplifying the corresponding signal. This low-noise detector is very transparent to neutrons and γ-rays, thus minimizing the background associated to neutron reactions in the structural materials and the absorption of the γ-rays emitted in the neutron-induced reactions. The MGAS signals are first preamplified and then connected to similar digitizers, in this case with a sampling rate of 100 MHz (because the signals are slower than those of BaF_2) and thus allowing the record of 80 ms long data buffers that cover the neutron energy range down to 20 meV.

A picture of the set-up combining both detectors is shown in fig. 2. The MGAS detectors were mounted in the center of the TAC, at 3 mm distance between each other and inside a sealed beam tube filled with gas: He+2% isobutane at atmospheric pressure. Each MGAS detector, with an active area of 3.5 cm in diameter, was loaded with a ^{235}U sample of 2 cm in diameter and 1.02(1) mg in mass, thus with a surface density of 324(3) μg/cm^2. The uranium sample, with an isotopic purity of 99.94%, where prepared by evaporation onto a mylar foil in the *Institute for Reference Materials and Measurements* [11].

3 Detector response and analysis in coincidence

3.1 Detector signals from TAC and MGAS

The γ-ray signals from the BaF_2 crystals of the TAC are characterized by a very fast (0.7 ns) and a slow (630 ns) scintillation component (see top panel in fig. 4), carrying each approximately 15% and 85% of the total light output, respectively. The combination of the very fast scintillation component and the sampling rate of 250 MHz provide a time resolution better than 4 ns. However, due to the uncertainty in the time calibration of the digitizer's internal clocks the overall time resolution of the TAC when all modules are analyzed in coincidence decreases down to 10 ns.

The characteristics of the MGAS signals are determined by the geometry of the detector as well as by the

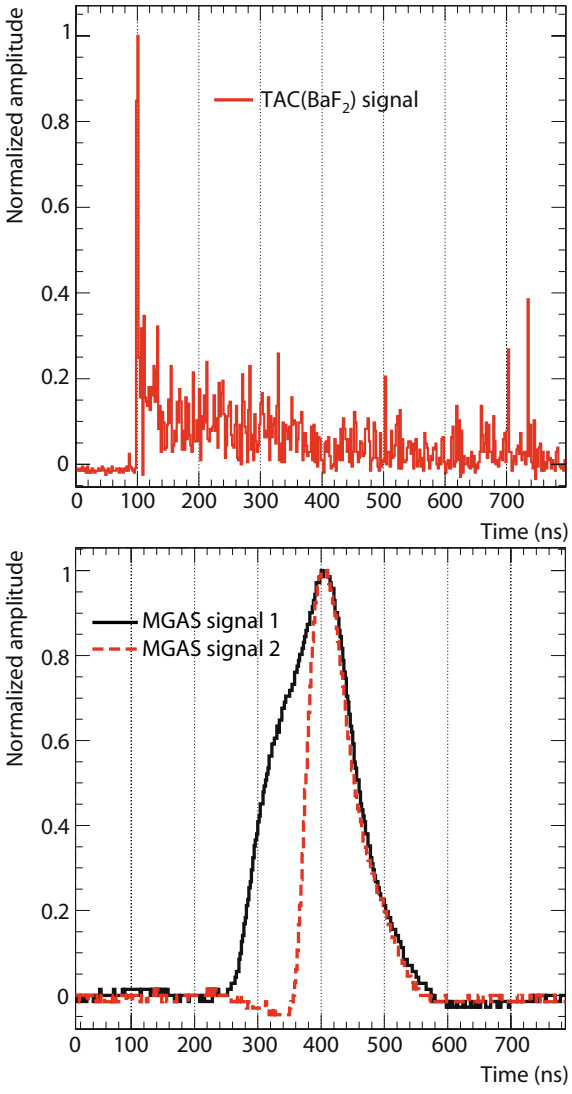

Fig. 4. Typical signals from the TAC (top panel) and MGAS (bottom panel) detectors. See text for a detailed discussion on the differences between the two MGAS signals.

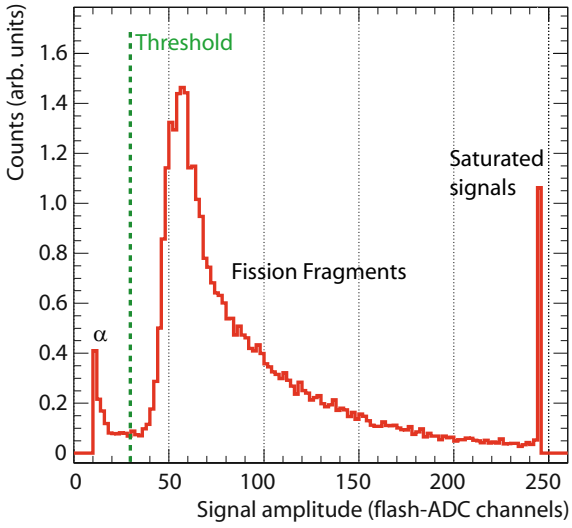

Fig. 5. Pulse height distribution of one of the MGAS detectors. The dashed vertical line corresponds to the threshold applied to distinguish between signals associated to α particles and fission fragments. The sharp edge at channel 248 corresponds to saturated signals, that is with an amplitude larger than the range of the 8 bit flash-ADC.

gas and electronics chosen. In this work, helium has been chosen instead of argon (or Ar+CF_4) because of its lower neutron cross-section that helps to reduce the background induced in the TAC. The drawback is a slower drift velocity of the electrons with respect to argon [12].

Two MGAS signals are illustrated in the bottom panel in fig. 4, showing that the typical rise times are in the range 50 to 150 ns. It is observed in the figure that signal 1 is broader than signal 2 due to a much slower rise time, which happens when the fission fragments are emitted at very low angles with respect to the sample surface and thus travel up to a few cm through the gas, sometimes without reaching the mesh. In such cases, most electrons are produced a few mm away from the mesh and need a larger drift time to reach the amplification region of the detector (at 4 mm distance). As a consequence of the longer drift time, the signals are produced with a slower rise time and hence result in a worse time resolution.

The signals from each detector are analyzed offline by dedicated pulse shape analysis routines that return the amplitude, integral and time of flight of each signal, the latter determined as in a Constant Fraction Discriminator (at 30% of the maximum amplitude). An example of the signal amplitude distribution for one of the MGAS detectors is shown in fig. 5, where the threshold that allows us to separate fission fragments (high amplitude) from α particles (low amplitude) is found around 30 flash-ADC channels.

In the neutron energy region of interest, around a few eV, the counting rates recorded in the detectors remained below 0.1 counts/μs (100 kHz) even at the peak of the resonances; meaning that problems related to pile-up and summing were negligible in both TAC and MGAS.

3.2 Analysis in coincidence of TAC and MGAS

Prior to the analysis of signals from the TAC and MGAS all the internal clocks of all the digitizer modules are synchronized with respect to one module used as a reference. The individual signals of the BaF_2 crystals are then grouped into *TAC events* using a coincidence window of 20 ns, resulting in a list of events characterized by the total energy E_{sum} deposited in the TAC and the number m_{cr} of crystals hit, referred to as crystal multiplicity. The time of the first detected γ-rays is also used to extract the time of flight and, consequently, the neutron energy.

For each signal detected in any of the MGAS detectors, a loop runs over the TAC events selecting those with a TOF_{TAC} between $\mathrm{TOF}_{MGAS} - 300$ ns and $\mathrm{TOF}_{MGAS} + 50$ ns (the asymmetry of this selection is explained later in the text). In 60% of the coincidences there is a single TAC event candidate inside such time interval, whereas two or three candidates are found in 30% and 7% of the cases, respectively. When there is more than one candidate, the fission events are discriminated efficiently from the background because of their higher multiplicity and energy (the background candidates have a multiplicity close to 1 and energies of a few hundred keV). The algorithm identifies the fission event as the one with the largest multiplicity and the largest energy deposition. In this way, a coincident event is found in the TAC for 97% of the MGAS fission events. This value corresponds to the TAC efficiency for detecting fission events in coincidence with the MGAS and such events are marked as *fission tagged*.

The time distribution between fission events in the MGAS and the TAC is displayed in fig. 6. The distribution shows two well-distinguished regions: a symmetric peak around 0 ns (FWHM$\sim$ 20 ns) containing 80% of

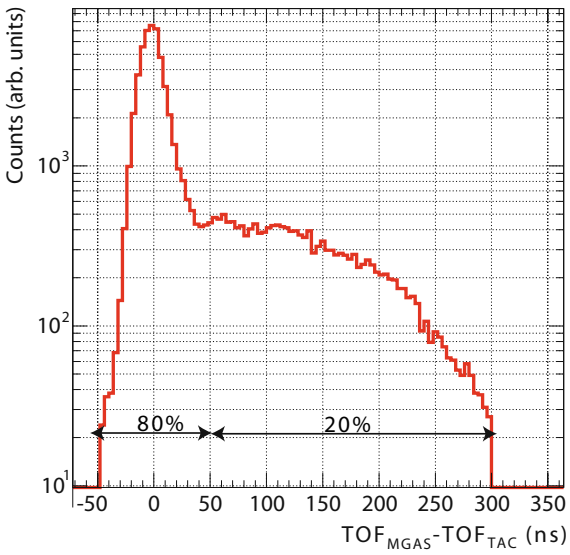

Fig. 6. Time difference between fission events detected in the MGAS and the TAC. The coincidence window for the analysis corresponds to the range TOF_{MGAS}–$\mathrm{TOF}_{TAC} \in [-50\,\mathrm{ns}, +300\,\mathrm{ns}]$.

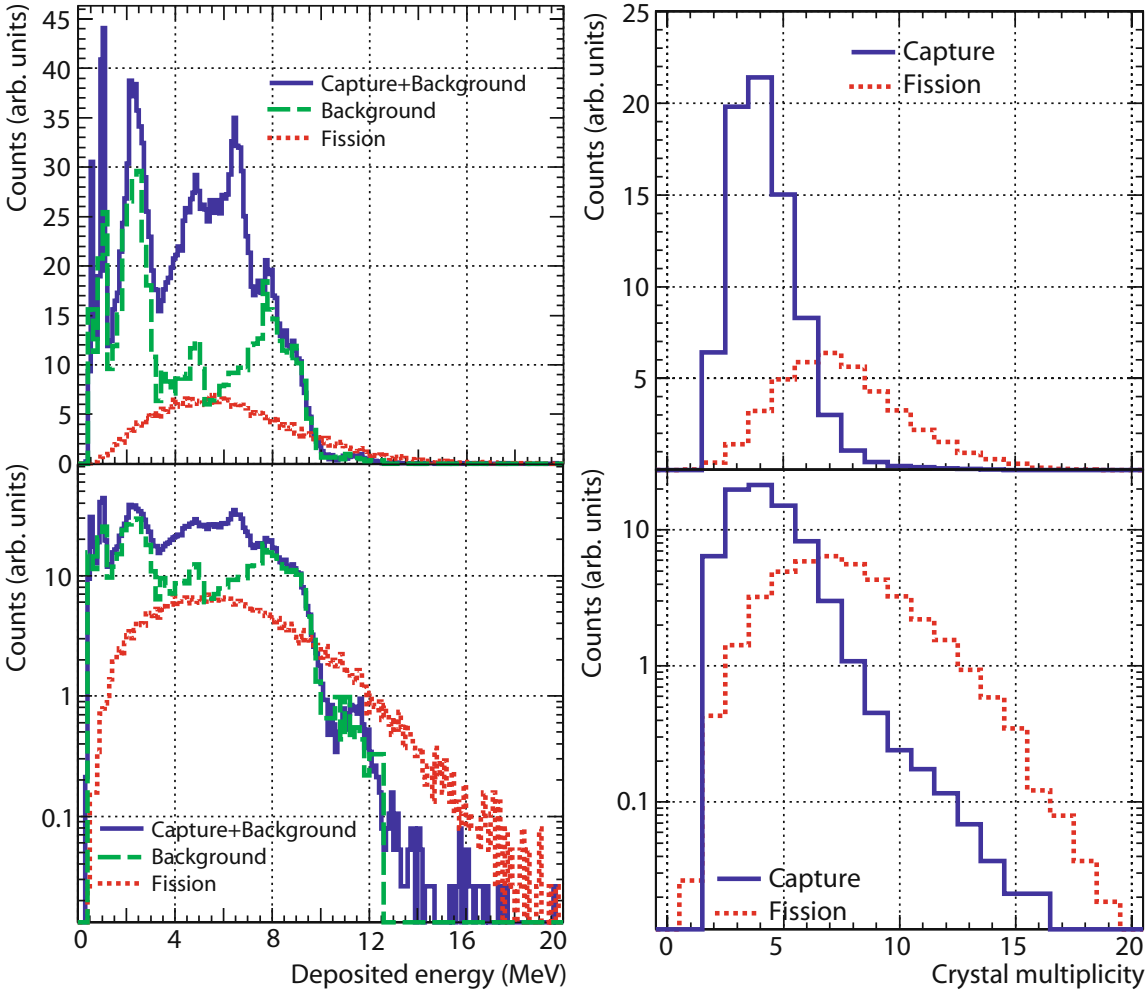

Fig. 7. (Color online) Left: Distributions of deposited energy corresponding to fission (red), capture+background (blue), and background (green) in linear (top) and logarithmic (bottom) scales. Right: Distributions of crystal multiplicity for events with $E_{sum} > 3$ MeV corresponding to fission (red) and capture (blue) in linear (top) and logarithmic (bottom) scales. The capture (blue) events are obtained by subtraction of the *Background* from the *Capture+Background* distribution shown in the left panel.

the events, and a tail at longer times containing all other events. The cumulative number of events amounts to 80%, 87%, 97% and 99.8% for $\Delta t = 50$, 100, 200 and 300 ns, respectively. The symmetric contribution corresponds to fission fragments emitted at small angles with respect to direction of the neutron beam, which reach the mesh within a few ns so that the electrons are collected very rapidly. On the contrary, the tail is related to fission fragments emitted at large angles as discussed in the previous section. This tail could be minimized by using a geometry with a thinner drift region and also by adding a few percent of CF_4 to the gas mixture, which would increase the drift velocity of the electrons.

3.3 Response of the TAC to fission and capture reactions

The response of the TAC to all events in terms of observed deposited energy and multiplicity distributions is shown in fig. 7. In order to minimize the background, the spectra in the figure have been constructed with a condition on neutron energy between 1 and 20 eV (*i.e.* 3.0 < TOF (ms) < 13.4), a region in which several strong resonances are present in the capture and fission cross-section of ^{235}U. The background spectrum shown in the figure has been obtained by a dedicated measurement without the ^{235}U samples.

The left panel in fig. 7 shows the deposited energy distributions of capture, fission and background events. The plot illustrates significant differences between the TAC responses to different types of reactions. The spectrum for capture events is limited to energies below 7 MeV and is dominated by the structure at $S_n(^{236}U) \sim 6.6$ MeV corresponding to the total absorption of γ-ray cascades from ^{235}U(n,γ) reactions. On the contrary, the fission distribution shows a smooth behavior peaking around 5 MeV and ranging up to 15–20 MeV, well above the total absorption peak of capture. The structures observed in the background measurement are caused mainly by the activity of the crystals ($E_{sum} < 4$ MeV) and by neutron capture reactions in the BaF_2 crystals (see [8] for details).

The crystal multiplicity distributions for events with $E_{sum} > 3\,\text{MeV}$ are shown in the right panel in fig. 7. The capture events are characterized by relatively low multiplicities compared to fission events, whose multiplicity distribution peaks around 7 and ranges up to 20, indicating that as much as half of the TAC is firing.

The differences in the TAC response to fission and capture events are a powerful tool to learn about the physics behind the processes, for instance, by comparing the experimental results with expectations from models of fission fragment distributions and electromagnetic decay, including information on Photon Strength Functions [13]. Such differences are also very useful for separating the capture and fission contribution when analyzing the fission and capture data, respectively, by imposing conditions on the deposited energy and crystal multiplicity. This is illustrated in fig. 7 where, for instance, all events observed at $E_{sum} > 10\,\text{MeV}$ or $m_{cr} > 10$ clearly correspond only to fission reactions and can therefore be neglected in the analysis of the capture events.

4 Determination of the detection efficiencies

With two detectors and two different reactions to detect, it is important to determine with high accuracy the different efficiencies that play a role in the measurement and their interrelations. Because capture reactions are only detected in the TAC, the efficiency $\varepsilon_{TAC}(n,\gamma)$ is independent of the use of the fission tagging technique. On the contrary, when a fission reaction occurs, there are four possibilities: i) the event is detected in both detectors, ii) in none of them, iii) only in the MGAS, and iv) only in the TAC.

In the calculations that follow, it is assumed that the efficiencies of the TAC and MGAS are equal for reactions occurring in any of the three MGAS detectors, separated only 15 mm from each other.

4.1 Detection efficiency of the MGAS: $\varepsilon_{\mathsf{MGAS}}(\mathsf{n,f})$

The efficiency for detecting fission events from the ^{235}U samples in the MGAS has been determined experimentally. Three reasonable assumptions are made regarding the high-multiplicity and/or high-energy events in the TAC: i) they are only due to fission (see fig. 7), ii) the efficiency of the TAC for detecting them is $\sim 100\%$ (see the next section and details in ref. [14]), iii) regarding their detection in the MGAS, these fission events are representative for all the events seen by the MGAS.

Based on these assumptions, the detection efficiency of the MGAS is calculated as the ratio of fission tagged to all TAC events for multiplicities larger than 10. The mentioned ratio is shown in fig. 8 for two different conditions in the variable deposited energy: $E_{sum} > 3\,\text{MeV}$ and $E_{sum} > 7\,\text{MeV}$. Under the first condition there could be both capture and fission events while only fission events fulfill the second condition (see left panel in fig. 7). However, in both cases the ratio above $m_{cr} = 10$ is constant and yields the same value: $\varepsilon_{MGAS}(n,f) = 0.90(2)$, where the uncertainty corresponds to the level of the fluctuation of the two distributions shown in fig. 8 above multiplicity 10.

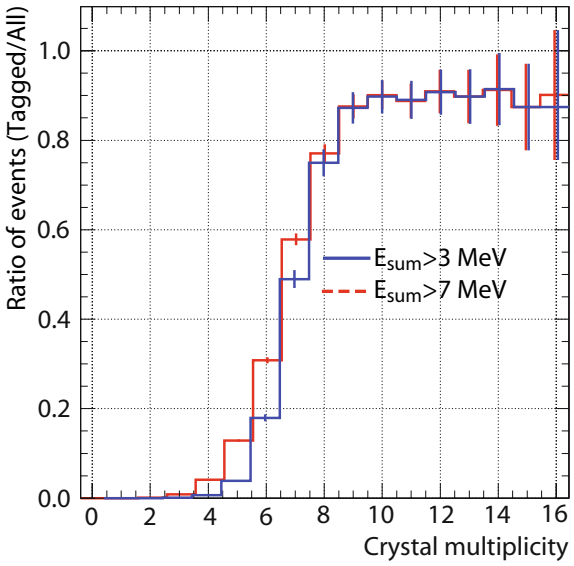

Fig. 8. Ratio of TAC events identified as fission *versus* all the detected events. The blue and red lines correspond to different analysis conditions, $E_{sum} > 3\,\text{MeV}$ and $E_{sum} > 7\,\text{MeV}$, respectively. The constant value for $m_{cr} > 10$ is $\varepsilon_{MGAS}(n,f) = 0.90(2)$.

4.2 Detection efficiency of the TAC for fission events: $\varepsilon_{\mathsf{TAC}}(\mathsf{n,f})$

As mentioned in sect. 3.2, a coincident event in the TAC is found for 97% of the MGAS fission events, *i.e.* signals with amplitudes larger than 20 channels. This value, very close to 100%, corresponds to the TAC efficiency for detecting fission events $\varepsilon_{TAC}(n,f)$. However, the analysis of the TAC is always carried out under certain conditions on deposited energy and multiplicity in order to reduce the overall background, therefore the detection efficiency $\varepsilon_{TAC}(n,f)$ (*i.e.* the ratio of TAC coincidence to total MGAS events) has been determined for different conditions on deposited energy and multiplicity, yielding the values listed in table 1. The large reduction of $\varepsilon_{TAC}(n,f)$ under the conditions $m_{cr} < 9$ and $E_{sum} < 7\,\text{MeV}$ allows reducing the background from fission reactions in the analysis of capture events, which are characterized by lower multiplicities (see fig. 7).

4.3 Detection efficiency of the TAC for capture events: $\varepsilon_{\mathsf{TAC}}(\mathsf{n},\gamma)$

The detection efficiency $\varepsilon_{TAC}(n,\gamma)$ can be calculated accurately by means of Monte Carlo simulations. We have demonstrated in a previous work [14] that using a GEANT4 [15] simulation it is possible to determine with good accuracy (2–3%) the detection efficiency $\varepsilon_{TAC}(n,\gamma)$

Table 1. Efficiency (in %) of the TAC for detecting fission events $\varepsilon_{TAC}(n,f)$ under different conditions on deposited energy and crystal multiplicity. The systematic uncertainty is estimated to be a unit in the last digit.

Energy	Crystal multiplicity							
(MeV)	>0	>1	>2	>3	1–9	2–9	3–9	4–9
>0	97	94	90	84	71	68	64	58
>1	93	93	90	83	67	67	64	57
>2	88	88	86	82	62	62	60	56
>3	80	80	79	77	54	54	53	51
0–7	65	62	58	52	58	56	52	45
1–7	61	62	58	51	55	54	51	45
2–7	56	56	54	50	49	49	48	43
3–7	48	48	47	45	41	41	40	38

for any condition on E_{sum} and m_{cr}, provided that the details on the detector geometry and the information available on the nuclear levels and transition probabilities of the compound nucleus formed after neutron capture are included in the simulation.

In this work we have done the same type of calculation, which returns the value $\varepsilon_{TAC}(n,\gamma) = 0.70(2)$ under the conditions $m_{cr} > 2$ and $3 < E_{sum}(\mathrm{MeV}) < 7$ chosen for the analysis.

5 Cross-sections and comparison to evaluations

5.1 Background subtraction

The fission rate measured in the MGAS is free of any background when the condition in signal amplitude is applied (see fig. 5). In the TAC, the capture contribution to the total measured counting rate is estimated by subtracting the contributions from fission and other backgrounds. Regarding the subtraction of the fission contribution to the TAC, as shown previously the MGAS has an efficiency for detecting fission reactions of 0.90, and thus the fission counting rate is scaled up by 0.90^{-1} before subtracting it from the TAC events. The remaining background component, which changes smoothly with increasing neutron energy, has been determined from a measurement in a similar configuration where the ^{235}U samples have been dismounted from the chamber (see left panel in fig. 7).

5.2 Calculation of the cross-sections

The capture and fission cross-sections $\sigma_{n,x}(E_n)$ are calculated from the measured yield under the assumption of the thin target approximation in which $Y_{n,x}(E_n) = n_{at} \cdot \sigma_{n,x}(E_n)$, where the equivalent thickness of the three ^{235}U samples together is $n_{at} = 8.32 \cdot 10^{-7}$ atoms/barn. Thus, the experimental cross-section is determined as

$$\sigma_{n,x}(E_n) = \frac{1}{n_{at}} \cdot \frac{C(E_n) - B(E_n)}{\varepsilon_{TAC}(n,x) \cdot \Phi(E_n) \cdot F_{BIF}}, \quad (1)$$

where $C(E_n)$ and $B(E_n)$ are the total and background counts, $\varepsilon_{TAC}(n,x)$ is the detection efficiency (different for fission and capture), $\Phi(E_n)$ is the incident neutron flux, and F_{BIF} is a scaling factor that corresponds to the fraction of the incident beam (3.7 cm in diameter) intercepted by the samples (2 cm in diameter). The latter, which is similar for fission and capture, can be estimated from the position of the sample and the knowledge on the beam profile, but it is more accurately determined as the value required for the calculated $\sigma(n,f)$ to match the ENDF/B-VII.0 evaluation, which is known within 1% in this energy range [16]. One can thus say that the measurement is normalized to the ENDF/B-VII.0 fission cross-section between 6 and 22 eV. In future measurements, the use of samples with larger diameter will eliminate the need of normalizing to an external reference (in this case the fission cross-section) because the full neutron beam will be incident on the samples.

5.3 Cross-sections and comparison to evaluations

The measured capture and fission cross-sections are displayed together with the evaluations in the two upper panels of fig. 9, where the evaluated cross-sections from ENDF/B-VII.0 (similar to all other evaluations) are shown for comparison. The ratio between the resonance integral of the capture and fission cross-sections obtained in this work and those from the ENDF/B-VII.0 evaluation are shown in the third panel. Last, the bottom panel shows a comparison between the α values of this work and those of the evaluations, where α is the ratio betwee the capture and fission cross-sections ($\alpha = \sigma_\gamma/\sigma_f$).

The comparison between the measured and evaluated cross-sections (two upper panels) shows an overall good agreement between measurement and evaluation for both types of reaction. Still at a qualitative level, one observes the absence of contamination from fission in the capture data and vice versa. The ratios displayed in the last two panels indicates that the tagging of fission events as well as the subtraction of the fission contribution, which includes the scaling by the detection efficiency $\varepsilon_{MGAS}(n,f)$, are accurate. Considering that the data have been normalized to the fission cross-section in the region of interest, the good agreement in the absolute value of the capture cross-section provides good evidence that the calculation of the detection efficiency $\varepsilon_{TAC}(n,\gamma)$ by Monte Carlo simulations is accurate.

The result shows that the combination of two efficient fission and capture detectors, when taking care of the interdependence with each other in the data analysis, allows the extraction of fission and capture cross-sections of fissile isotopes without ambiguity.

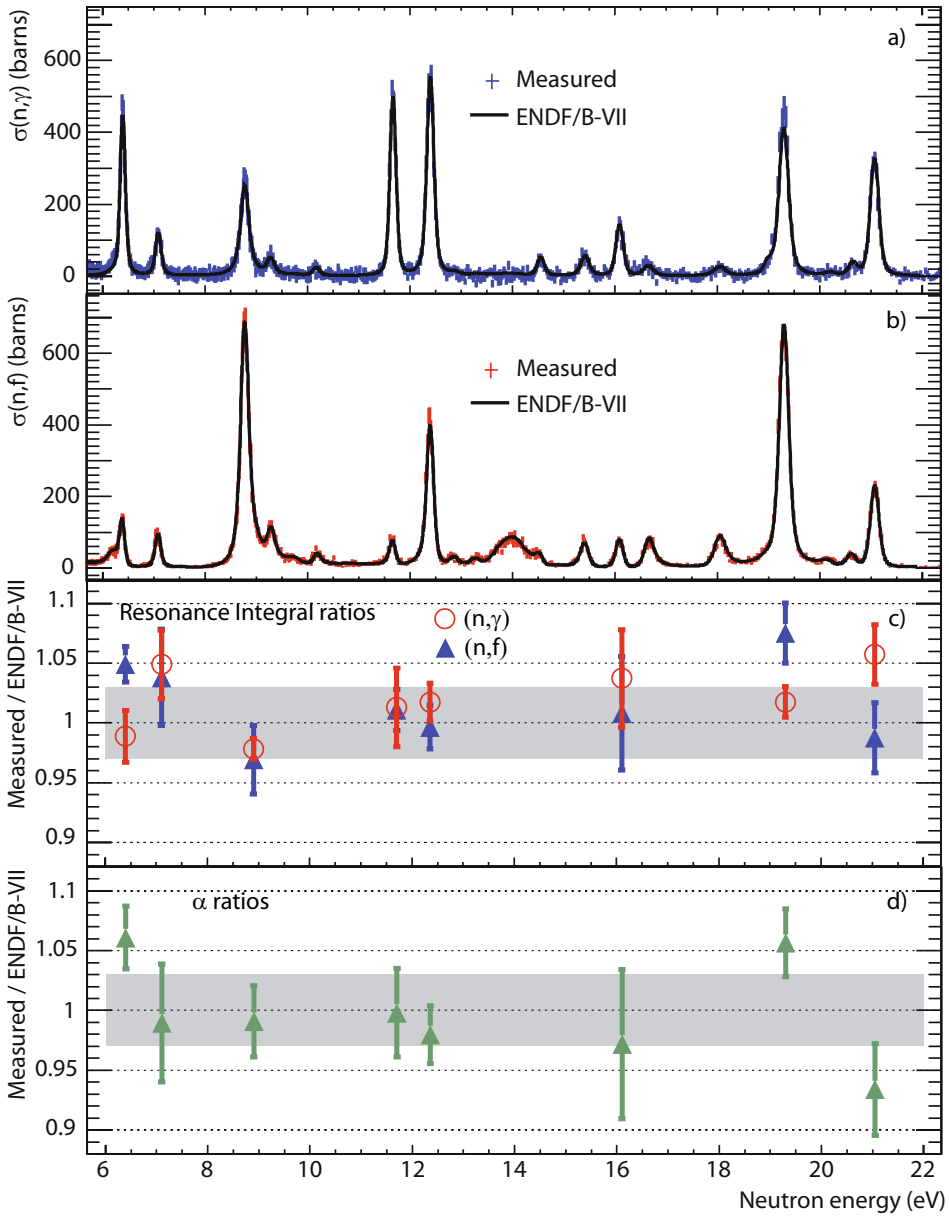

Fig. 9. (Color online) Overall comparison of the results from this work and the ENDF/B-VII.0 evaluated cross-sections. a,b) Experimental (red and blue histograms) and evaluated (black lines) capture and fission cross-sections. c,d) Ratio of measured and evaluated resonance integrals and α ($= \sigma_\gamma/\sigma_f$) ratios. The shaded areas in c) and d) indicate the region of agreement within $\pm 3\%$.

6 Conclusions

The measurement of capture cross-sections of fissile isotopes is of utmost importance in the field of nuclear technology but it poses a challenge from the experimental point of view: the γ-ray background emitted in fission reactions complicates the measurement of weaker γ-signals associated with (n,γ) reactions. We have built and tested a new set-up at the CERN n_TOF facility that allowed us to measure simultaneously neutron-induced fission and capture reactions by combining a 4π Total Absorption Calorimeter (TAC) with several MicroMegas (MGAS) detectors loaded with a total of 3 mg of ^{235}U.

A detailed analysis of the measured data including the optimization of the coincidence algorithm and the determination of the several detection efficiencies involved in the process has confirmed the successful and unambiguous identification of capture and fission events. The analysis of the extracted capture and fission cross-sections shows that the results are in good agreement with the ENDF/B-VII.0 evaluation in the energy region under study (6–22 eV).

In view of the present results, a new experimental campaign is envisaged at n_TOF for measuring capture cross-sections of fissile isotopes such as ^{233,235}U, ^{239,241}Pu and ^{245}Cm, always considering the very limited availability of suitable samples. The first measurement using ~ 30 mg of ^{235}U is scheduled for 2012 [17].

The authors are indebted to Damien Grenier and Vincent Barozier, the CERN TE-MPE-EM group, and IRMM for their work on the manufacturing of the fission chamber, the MicroMegas detectors and the ^{235}U samples, respectively. This work was supported in part by the Spanish national company for radioactive waste ENRESA, through the CIEMAT-ENRESA agreements on "Transmutación de residuos radiactivos de alta actividad", the Spanish Plan Nacional de I+D+i de Física de Partículas (project FPA2008-04972-C03-01), the Spanish Ministerio de Ciencia e Innovación through the CONSOLIDER CSD 2007-00042 project and the European Commission 7th Framework Programme project ANDES (PN-249671).

References

1. A.J. Koning , J. Blomgren, R. Jacqmin, A.J.M. Plompen, R. Mills, G. Rimpault, E. Bauge, D. Cano-Ott, S. Czifrus, K. Dahlbacka, I. Goncalves, H. Henriksson, D. Lecarpentier, E. Malambu-Mbala, V. Stary, C. Trakas, C. Zimmerman, *CANDIDE: Nuclear data for sustainable nuclear energy* (2009) EUR 23977 EN.
2. Working Party on International Evaluation Co-operation of the NEA Nuclear Science Committee, *Uncertainty and target accuracy assessment for innovative systems using recent covariance data evaluations*, (2008) ISBN 978-92-64-99053-1.
3. NEA Nuclear Data High Priority Request List, `http://www.nea.fr/dbdata/hprl/index.html`.
4. U. Abbondanno *et al.*, *CERN n_TOF Facility: Performance Report*, CERN-SL-2002-053 ECT.
5. E. Gonzalez-Romero *et al.*, *Measurement of the neutron capture cross sections of ^{233}U, $^{240,242}Pu$, $^{241,243}Am$ and ^{245}Cm with a Total Absorption Calorimeter at n_TOF*, (2003) CERN-INTC-2003-036, INTC-P-182.
6. D. Cano-Ott, F. Gunsing *et al.*, *Neutron capture cross section measurements of ^{238}U, ^{241}Am and ^{243}Am at n_TOF*, (2009) CERN-INTC-2009-025, INTC-P-269.
7. E. Berthoumieux *et al.*, *Simultaneous measurement of the neutron capture and fission yields of ^{233}U*, in *Proceedings of the International Conference on Nuclear Data for Science and Technology April 22–27, 2007, Nice, France* (EDP Sciences, 2008) pp. 571–574, DOI: 10.1051/ndata:07665.
8. C. Guerrero *et al.*, Nucl. Instrum. Methods A **608**, 424 (2009).
9. S. Andriamonje *et al.*, J. Korean Phys. Soc. **59**, 1597 (2011).
10. T.A. Bredeweg *et al.*, Nucl. Instrum. Methods B **261**, 986 (2007).
11. `http://irmm.jrc.ec.europa.eu`.
12. J. Pancin, *Détection de Neutrons avec un Détecteur de Type Micromegas: de la Physique Nucléaire à l'Imagerie*, PhD Thesis, Université de Bordeaux, France (2004).
13. C. Guerrero *et al.*, J. Korean Phys. Soc. **59**, 1510 (2011).
14. C. Guerrero *et al.*, Nucl. Instrum. Methods A **671**, 108 (2012).
15. S. Agostinelli *et al.*, Nucl. Instrum. Methods A **506**, 250 (2003).
16. K. Shibata, J. Nucl. Sci. Technol. **42**, 130 (2005).
17. C. Guerrero, E. Berthoumieux, D. Cano-Ott, *Measurements of neutron-induced capture and fission reactions on ^{235}U: cross sections and α ratios, photon strength functions and prompt γ-ray from fission*, (2011) CERN-INTC-2011-045 INTC-P-309.